

3-Amido Pyrrolopyrazine JAK Kinase Inhibitors: Development of a JAK3 vs JAK1 Selective Inhibitor and Evaluation in Cellular and in Vivo Models

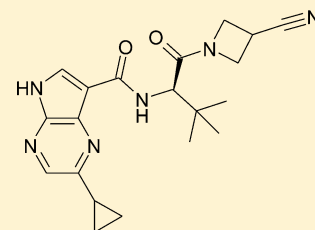
Michael Soth,^{*,†} Johannes C. Hermann,[†] Calvin Yee,[†] Muzaffar Alam,[†] Jim W. Barnett,[‡] Pamela Berry,[†] Michelle F. Browner,[‡] Karl Frank,[‡] Sandra Frauchiger,[‡] Seth Harris,[‡] Yang He,[†] Mohammad Hekmat-Nejad,[‡] Than Hendricks,[‡] Robert Henningsen,[‡] Ramona Hilgenkamp,[†] Hoangdung Ho,[‡] Ann Hoffman,[†] Pei-Yuan Hsu,[†] Dong-Qing Hu,[†] Andrea Itano,[‡] Saul Jaime-Figueroa,[†] Alam Jahangir,[‡] Sue Jin,[†] Andreas Kuglstatler,[†] Alan K. Kutach,[‡] Cheng Liao,[†] Stephen Lynch,[†] John Menke,[†] Linghao Niu,[†] Vaishali Patel,[†] Aruna Railkar,[†] Douglas Roy,[†] Ada Shao,[‡] David Shaw,[‡] Sandra Steiner,[†] Yongliang Sun,[†] Seng-Lai Tan,[†] Sandra Wang,[‡] and Minh Diem Vu[†]

[†]Hoffmann-La Roche, 340 Kingsland Street, Nutley, New Jersey 07110, United States

[‡]Roche Palo Alto, 3431 Hillview Avenue, Palo Alto, California 94304, United States

S Supporting Information

ABSTRACT: The Janus kinases (JAKs) are involved in multiple signaling networks relevant to inflammatory diseases, and inhibition of one or more members of this class may modulate disease activity or progression. We optimized a new inhibitor scaffold, 3-amido-5-cyclopropylpyrrolopyrazines, to a potent example with reasonable kinome selectivity, including selectivity for JAK3 versus JAK1, and good biopharmaceutical properties. Evaluation of this analogue in cellular and in vivo models confirmed functional selectivity for modulation of a JAK3/JAK1-dependent IL-2 stimulated pathway over a JAK1/JAK2/Tyk2-dependent IL-6 stimulated pathway.

**■ INTRODUCTION**

The Janus kinase family members (JAK3, JAK2, JAK1, and TYK2) play critical and cooperative roles in transmitting many signaling cascades in response to inflammatory and proliferative signals. For instance, JAK3 acts in concert with JAK1 to relay cytokine signaling through the cytokine receptor common γ chain, also known as CD132.^{1,2} Null mutations in either JAK3 or CD132 are associated with severe combined immunodeficiency (SCID) disorder.^{3–5} JAK2 is important in the signaling of hormones and growth factors such as erythropoietin (EPO), through the EPO receptor, as well as granulocyte-macrophage colony stimulating factor (GM-CSF) via its receptor and the common β chain IL-3 receptor.^{6,7} JAK1, JAK2, and TYK2 are involved in IL-6 signaling.^{8–10} Across the pharmaceutical industry, there is high interest in targeting the JAK family of kinases for both oncology and inflammation indications.^{11–15} Within the inflammation arena, Pfizer's Tofacitinib, **1** (Figure 1), a JAK3/2/1 inhibitor initially reported as a selective JAK3 inhibitor, has shown promising efficacy results in clinical trials for rheumatoid arthritis (RA).^{16,17}

However, it is unclear if blockade of all JAK isozymes is required for optimal efficacy without compromising the risk/benefit profile or if a more isozyme-selective inhibitor would suffice. There are divergent opinions in the literature as to the functional consequences of selective inhibition of JAK3 over JAK1. Recent papers from the Novartis group have questioned whether this type of selectivity profile will be sufficient to

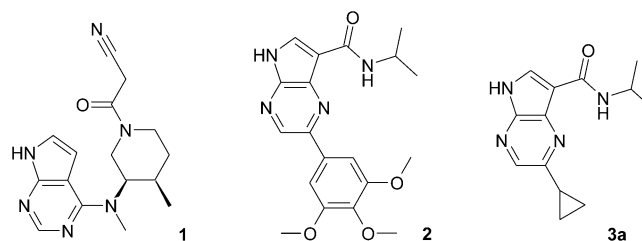


Figure 1. Structures of Tofacitinib (**1**), profiling hit **2**, and cyclopropyl analogue **3a**.

efficiently block immunologically relevant pathways mediated by CD132 cytokines.^{18,19} The Novartis group reached this conclusion on the basis of cellular data on a highly JAK3-selective compound compared to Tofacitinib **1**, coupled with extensive biological studies dissecting the roles of JAK3 and JAK1 in IL-2-induced STAT5 phosphorylation (a CD132-dependent process). However, an earlier paper from the Pharmacoepia/Wyeth/Pfizer group concluded that JAK1 inhibition is not required for potent inhibition of IL-2 signaling, and with a JAK3-selective tool compound they demonstrated potent, selective inhibition of IL-2 signaling over cellular pathways requiring JAK-family enzymes other than JAK3.²⁰ Thus, it would be important

Received: November 7, 2012

Published: December 9, 2012

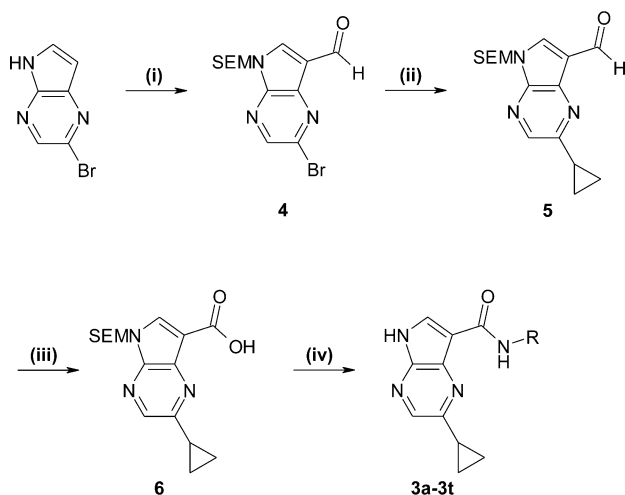
to resolve this discrepancy using structurally distinct scaffolds of JAK inhibitors.

Our JAK medicinal chemistry program strategy was to explore a diverse range of series with varying JAK family selectivity profiles as tool compounds to dissect the relative role of each JAK member in inflammatory disease indications. Here, we describe the optimization of a 3-amido-5-cyclopropyl pyrrolopyrazine series to potent JAK inhibitors, culminating in an example with selectivity for JAK3 over JAK1 and properties conducive to oral dosing and testing in an acute PK/PD mouse model. Our optimized compound shows both cellular and in vivo selectivity for inhibition of an IL-2 signaling pathway, most notably against an IL-6 receptor mediated signaling pathway. In addition, the structure–activity relationships (SAR) around close analogues indicate that improved selectivity for JAK3 over JAK1 does not result in a decrease in potency for inhibition of the IL-2 signaling pathway.

RESULTS AND DISCUSSION

Chemistry. The general synthetic scheme for the preparation of 3-amido-5-cyclopropyl pyrrolopyrazines is shown in Scheme 1. Commercially available 5-bromopyrrolopyrazine was con-

Scheme 1. General Synthesis of Pyrrolopyrazines 3a–t^a



^aReagents and conditions: (i) (a) formaldehyde, sodium hydroxide, 1,4-dioxane/water, (b) sodium hydroxide, tetrahydrofuran/water, (c) Jones reagent, acetone, (d) 2-silylethoxymethyl chloride, sodium hydride, *N,N*-dimethylformamide, 0 °C→rt, (42%); (ii) cyclopropylboronic acid, palladium diacetate, tricyclohexylphosphine, potassium phosphate, toluene/water, 100 °C (81%); (iii) sodium hypochlorite, potassium dihydrogen phosphate, sulfamic acid, 1,4-dioxane/water (87%); (iv) (a) *R*¹-NH₂, amide coupling reagent, solvent, (b) trifluoroacetic acid, dichloromethane, (c) ethylene diamine/dichloromethane or sodium acetate/ethanol or triethylamine/MeOH/H₂O (17–87%).

verted in a four-step process to silylethoxymethyl (SEM)-protected aldehyde **4**. Aldehyde **4** was subjected to Suzuki conditions to afford cyclopropyl analogue **5**. Oxidation of the aldehyde moiety afforded acid **6**, which was coupled to a variety of amines followed by SEM deprotection to afford final compounds **3a–t**.

Initial Hit and Optimization. The chemical starting point for this work came from a scan of our internal collection of kinase inhibitors for which we have kinome selectivity information. Inhibitor sets annotated by selectivity profiles can be a fruitful

source of leads for new kinase programs.²¹ The “hit” that we decided to pursue was pyrrolopyrazine **2**, which had been profiled by Kinomescan (now a division of DiscoverRx, formerly a division of Ambit Biosciences)²² and showed binding to JAK3, JAK2 and JAK1; however, it showed poor kinome selectivity.²³ Exploration of trimethoxyphenyl replacements afforded multiple subseries with varying kinome selectivities. This article describes the cyclopropyl subseries.

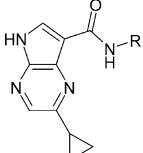
Replacement of the trimethoxyphenyl group of **2** with a cyclopropyl group to afford **3a** resulted in a reasonably potent JAK inhibitor (Table 1, first entry). We modeled **3a** into the ATP-binding site of JAK3 and looked for promising vectors to improve potency and possibly kinome selectivity (Figure 2). As both methyls of the amide isopropyl group point toward apparent pockets, we focused our SAR work on further derivatization of these two vectors (Table 1). During our efforts on this program, the crystal structure of **1** was obtained (and later published by others²⁴), showing space-filling of these pockets. SAR studies around **1** confirmed that these pockets are indeed excellent areas of the protein to fill for potency.²⁵ For the examples in this pyrrolopyrazine series, potency trends are similar across JAK isozymes, with many examples showing some preference for inhibiting JAK3 versus JAK2 and JAK1.

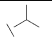
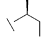
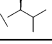
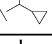
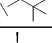
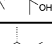
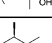
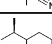
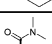
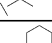
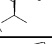
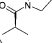
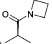

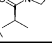
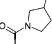
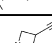
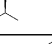
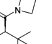
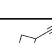
As shown in Figure 2, the “lower” pocket is defined in part by leucine (Leu956) and alanine (Ala966) residues. We therefore targeted this region with small hydrophobic groups off of the isopropyl amide (Entries **3b–3i**). A significant boost in potency was gained by simply replacing the lower methyl group with an ethyl (entry **3b** vs **3a**). Further elaboration to isopropyl and racemic cyclopropyl analogues (**3c** and **3d**) did not improve potency further; however, *tert*-butyl analogue **3e** showed an additional potency boost, bringing the potency down to a 1 nM compound. Replacing one methyl of the *tert*-butyl group with a hydroxyl group (**3f**) resulted in a significant potency loss; a nitrile replacement (**3h**) was more favorable. A cyclohexyl analogue (**3i**) was tolerated but less potent than the other examples from this exercise to fill the lower pocket. A crystal structure of analogue **3e** in JAK3 showed excellent space-filling of the lower pocket by the *tert*-butyl group (Figure 3).

Beyond potency considerations, the other noteworthy effect of filling the lower pocket is an improved selectivity for JAK3 versus JAK1. The larger groups (*tert*-butyl analogues and cyclohexyl) show 10–50-fold selectivity.

Interestingly, the hydroxyl-containing enantiomers **3f** and **3g** showed similar potencies against JAK3 (Table 1). Crystal structures for both of these compounds bound to JAK3 were obtained and showed a similar space-filling, i.e., the ligands were free to shift in the pocket to obtain optimal binding (Figure 4).

For the second vector, leading to the “upper pocket”, a modeling exercise highly prioritized a bis-amide motif as having low energy conformations most likely to fill the space available. The first simple examples **3j–m** did not show potency improvements over the parent **3a**; however, a crystal structure of compound **3k** (Figure 5) confirmed the expected binding motif and encouraged us to try further substitution, specifically with nitrile side chains, as a nitrile group in this pocket was observed to be particularly beneficial for potency by the Pfizer group in their development of compound **1**.²⁵ The nitrile group is also beneficial for our series (examples **3n**, **3p**). Comparison of methyl analogue **3o** to cyano analogue **3n** suggests that the potency boost is not due to simple space-filling. A recent paper from the Pfizer group attempts to explain the potency benefits of a nitrile group in this area of the protein.²⁴ For our scaffold, the

Table 1. Enzyme Potencies^a


Compound	R	JAK3 IC ₅₀ (nM) ^b	JAK2 IC ₅₀ (nM) ^b	JAK1 IC ₅₀ (nM) ^b
3a		44.5 ± 7.6	106.2 ± 6.3	224.3 ± 60.0
3b		9.6 ± 3.5	44.3 ± 5.9	75.8 ± 21.0
3c		7.8 ± 1.2	32.6 ± 2.5	44.8 ± 7.0
3d		8.6 ± 1.4	22.4 ± 3.2	24.0 ± 2.3
3e		1.4 ± 0.3	10.8 ± 2.3	44.5 ± 8.3
3f		17.0 ± 3.4	76.7 ± 11.7	256.7 ± 40.6
3g		19.0 ± 6.2	43.0 ± 1.0	99.7 ± 11.7
3h		1.8 ± 0.4	10.9 ± 3.0	108.1 ± 15.1
3i		43.6 ± 12.9	355.2 ± 47.3	1102.5 ± 224.9
3j		104.4 ± 8.2	231.2 ± 6.7	636.6 ± 184.7
3k		68.9 ± 23.3	123.1 ± 30.2	361.0 ± 20.4
3l		48.5 ± 5.2	121.6 ± 7.6	430.5 ± 185.8
3m		148.0 ± 24.3	345.4 ± 19.0	870.7 ± 111.2
3n		8.7 ± 0.7	23.1 ± 4.3	44.7 ± 12.4
3o		80.6 ± 11.3	134.2 ± 20.9	272.0 ± 41.8
3p		8.2 ± 1.1	36.8 ± 4.6	47.0 ± 15.6
3q		0.26 ± 0.09	0.80 ± 0.15	3.2 ± 1.1
3r		<0.4	<0.6	<0.5
3s		<0.3	<0.3	0.47 ± 0.02
3t		0.44 ± 0.04	0.50 ± 0.09	0.59 ± 0.06
1		2.2 ± 0.6	4.0 ± 0.7	1.6 ± 0.1

^aInhibition of phosphorylation of a biotinylated synthetic peptide catalyzed by JAK1–3; see Experimental Section for details. All enzyme reactions were run at adenosine triphosphate (ATP) concentrations of 1.5 μM. *K_m*s of these enzymes for ATP under our experimental conditions were determined to be 1.5 μM (JAK3), 6 μM (JAK2), and 20 μM (JAK1). ^bMean ± SEM (standard error of the mean), *n* ≥ 3 except for 3g and 3t (*n* = 2).

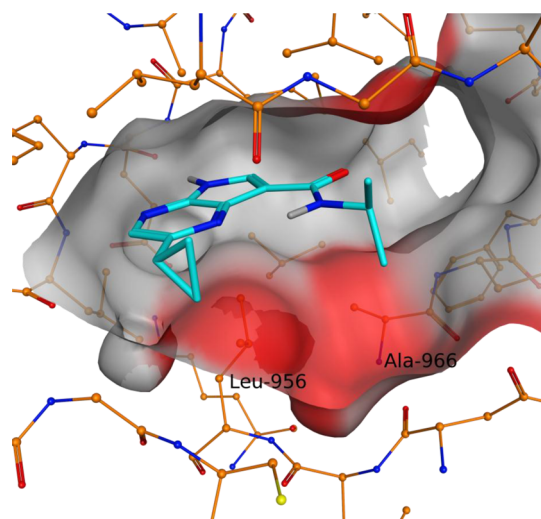


Figure 2. Modeled structure of 3a in JAK3. Carbon atoms of 3a are in cyan, carbon atoms of the JAK3 protein are in orange, oxygen atoms are in red, and nitrogen atoms are colored in blue. Red-colored protein surface indicates protein areas identified for potential exploration and optimization of interactions. All visualizations generated with MOE.²⁶

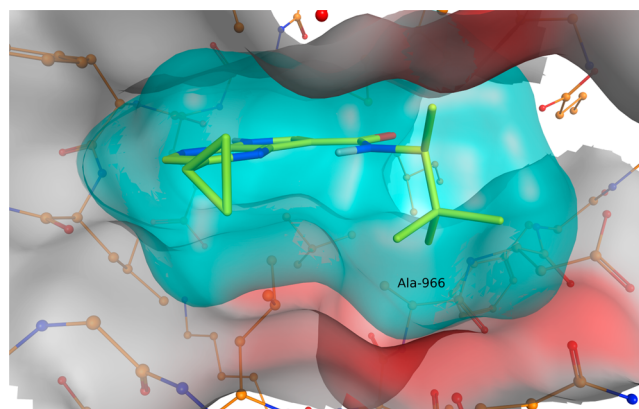


Figure 3. X-ray crystal structure of 3e in JAK3 (PDB accession no. 4HVD, 1.85 Å resolution), demonstrating filling of the lower pocket by the *tert*-butyl group. Carbon atoms of 3e are in yellow, carbon atoms of the JAK3 protein are in orange, oxygen atoms are in red, and nitrogen atoms are colored in blue. Molecular surface of 3e is colored cyan.

most promising side chains from this second exercise combined well with the most promising side chains of the first exercise (examples 3q–t), yielding highly potent inhibitors. The potencies of these compounds were comparable to Tofacitinib 1. Importantly, while compounds 3q–t all show similar potencies against JAK3, the *tert*-butyl example 3q is >10-fold selective against JAK3 while the cyclopropyl examples 3r–t are not selective against JAK1. This selectivity discrepancy among very closely related compounds allows for a useful interpretation of cellular data later in the manuscript.

Kinome Selectivity. We profiled our compounds by Caliper screening against a 48 kinase panel (Table 2). Caliper profiling measures percent inhibition of phosphorylation of a peptide substrate; the data in Table 2 is represented by heat maps, assigning <50% inhibition as completely green and >95% inhibition as completely red. We pick six examples here to

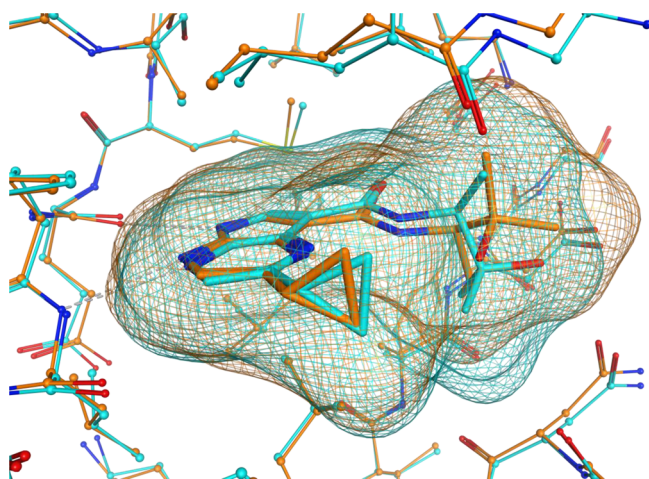


Figure 4. X-ray crystal structures of **3f** (PDB accession no. 4HVG, 2.75 Å resolution) and **3g** (4HVV, 2.3 Å) in JAK3, superimposed. Carbon atoms of **3f** are in cyan, carbon atoms of **3g** are in orange, oxygen atoms are in red, and nitrogen atoms are colored in blue. The assignment of methyl and hydroxyl in the tertiary alcohol moiety is tentative at the current resolution. Meshes are colored according to ligand carbon atom color and show the molecular surface for each ligand.

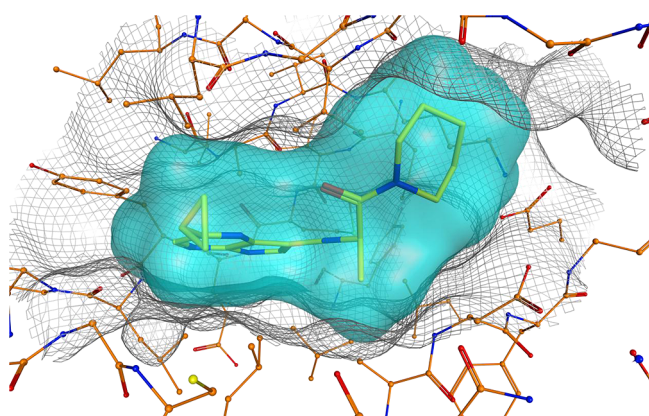


Figure 5. X-ray crystal structure of **3k** in JAK3 (PDB accession no. 4HVI, 2.4 Å resolution), demonstrating filling of the upper pocket by the tertiary amide. Carbon atoms of **3k** are in yellow, carbon atoms of the JAK3 protein are in orange, oxygen atoms are in red, and nitrogen atoms are colored in blue. Molecular surface of **3k** is colored cyan. Gray-colored mesh shows the molecular surface and shape of the binding site.

demonstrate the key selectivity learnings. For purposes of fair comparison, the concentration at which compounds were profiled reflects their JAK3 potency: for the less potent entries **3a** and **3f**, profiling was performed at 10 μM ; for the more potent entries **3e**, **3h**, and **3q**, profiling was performed at 1 μM . For entry **3p**, which has an intermediate potency, we include both 10 and 1 μM data.

Entries **3e** and **3h**, which fill the lower pocket with either the *tert*-butyl group or the closely related cyano analogue, show selectivity improvements relative to parent **3a**. These selectivity improvements are easily explainable by analysis of the protein in the areas filled. The lower pocket is in part defined by Ala966, which is a variable residue across the kinome and is often larger for other kinases, i.e., for other kinases there is not room for an optimal fit of the *tert*-butyl group. Indeed, the profiled kinases that are most strongly “hit” by entries **3e** and **3h** all contain alanine in this position.

It is more difficult to interpret the selectivity data for entry **3p**, which presumably fills the upper pocket with the cyanoazetidine amide group, because its JAK3 potency lies between that of **3a** and **3e/h** and so it is difficult to decide which analogue is the appropriate comparator. However, the upper pocket is mostly defined by a main-chain β -sheet, with side chains pointing away and unlikely to be key determinants of selectivity. What is clear is that the combination of the *tert*-butyl side chain with the cyanoazetidine amide is optimal for kinome selectivity (entry **3q**). The added selectivity of **3q** over **3e** does not necessarily mean that the cyanoazetidine group introduces specific binding interactions that favor JAK3. The added selectivity of **3q** over **3e** may simply be due to a tighter fit of a ligand optimized to JAK3 versus other kinases, i.e., the presence of the cyanoazetidine group restricts freedom of movement for the ligand within kinase pockets, disfavoring alternative ligand arrangements within other kinases. This idea is supported by the earlier noted observation that smaller ligands have freedom of movement within these pockets (Figure 4). Freedom of ligand movement could also explain the reduced selectivity of tertiary alcohol **3f** compared to **3e** and **3h**. The polar hydroxyl group of **3f** is likely more amenable to alternative, water-exposed binding conformations.

Cellular Activity and Biopharmaceutical Properties.

Select examples were tested in cell-based assays (Table 3). These assays measure the inhibition of phosphorylation of downstream signal transducer and activator of transcription (STAT) proteins, either in human peripheral blood mononuclear cells (PBMCs) or in human whole blood (HWB), upon treatment with varying stimuli (Table 3). The different cellular stimuli used induce phosphorylation of STATs by either dual JAK3/1 (IL-2 stimulus, STAT5a phosphorylation in T-cells), JAK2 (GM-CSF stimulus, STAT5a phosphorylation in monocytes), or dual JAK2/1 (IFN- γ stimulus, STAT1 phosphorylation in monocytes) containing pathways.

Only examples with high enzyme potency (10 nM or better) against at least one relevant isoform achieved sub- μM cellular potencies. Many of the compounds tested show cellular potencies comparable to those seen for compound **1**, although HWB potencies are less, presumably because of higher protein binding. For example, in our protein binding assays (human), compound **1** showed a free fraction of 99% while compound **3q** showed a free fraction of only 3%. Cellular selectivities within this panel are also comparable to those observed for **1**, with moderate selectivities seen for inhibition of IL-2 signaling versus GM-CSF and IFN- γ signaling.

Importantly, the examples with higher selectivity for JAK3 versus JAK1 still show potent inhibition of IL-2 signaling. Compound **3q** was equally potent in the IL-2 assay compared to its close analogue **3t**, which has a similar JAK3 enzyme potency but no selectivity against JAK1. These results cannot be explained by the cellular permeabilities of these compounds, which are comparable in our Caco-2 permeability assay (data not shown). We conclude that for these close comparators, loss of JAK1 potency did not affect potency in the IL-2 cellular assay and that a more selective inhibition of JAK3 catalytic function can be realized while still efficiently attenuating IL-2-induced STAT5a phosphorylation.

The *in vitro* biopharmaceutical properties for compounds in this series varied depending on the amide side chain. Our early screening funnel focused on solubilities and microsomal stabilities, which both tended toward low for purely aliphatic side chains and improved for more polar examples. At various stages in the optimization process, select compounds were more

Table 2. Kinome Selectivity Profiles for Select Examples^a

	3a (10 μM)	3e (1 μM)	3f (10 μM)	3h (1 μM)	3p (10 μM)	3p (1 μM)	3q (1 μM)
ABL	65	50	66	17	57	7	11
AKT1	16	-10	5	-2	-9	-9	-1
AKT2	9	-10	-12	3	-13	-8	-6
AMPK	91	83	93	37	90	36	67
AurA	89	90	95	55	93	33	78
BTK	7	6	3	13	18	1	3
CAMK2	13	22	42	-4	-17	-16	2
CAMK4	52	27	52	15	78	21	5
CDK2	92	84	95	81	96	65	44
CHK1	48	16	48	-6	38	-4	9
CHK2	90	51	90	7	92	33	11
CK1d	62	-1	2	-5	93	37	-2
c-Raf	42	12	44	-7	88	31	6
c-TAK1	73	49	90	-5	91	35	37
DYRK1a	67	45	55	38	67	17	5
Erk1	81	8	39	0	92	40	14
Erk2	62	6	32	-5	85	27	1
FGFR1	95	92	99	67	92	37	63
FLT3	46	49	62	-22	90	66	16
FYN	71	40	64	12	81	19	39
GSK3b	97	79	91	66	84	27	3
HGK	83	-5	56	-25	30	19	-3
IGF1R	-8	7	18	10	-8	0	-2
INSR	1	-1	9	-5	-13	5	-4
IRAK4	23	16	1	1	75	11	5
KDR	84	56	95	43	76	-6	8
LCK	64	43	67	3	82	16	49
LYN	63	32	59	0	91	31	57
MAPKAPK	84	72	86	6	25	3	2
MARK1	93	87	98	20	96	77	67
MET	24	3	19	-15	20	-8	-4
MSK1	28	16	54	3	39	2	2
MST2	98	99	99	81	93	33	36
p38a	7	-5	-5	0	-19	2	0
p70S6K	10	-11	17	-26	-17	1	8
PAK2	62	17	45	7	75	29	0
PIM2	-28	-14	3	-20	-27	-11	-7
PKA	49	11	53	-2	59	4	-10
PKCb	-22	1	10	9	3	1	-18
PKCz	16	-2	14	-1	14	1	-10
PKD2	82	76	75	-1	48	13	-1
PKGa	54	1	52	17	54	8	-4
PRAK	24	7	23	1	-3	-2	4
ROCK2	80	45	85	1	94	53	26
RSK1	95	42	84	1	80	17	8
SGK1	68	19	69	28	74	4	-5
SRC	59	37	74	1	85	23	57
SYK	-4	12	14	7	32	4	8

^a% inhibition of phosphorylation of substrates at the indicated test compound concentrations, using a ProfilerPro Kit 1 (P/N 760373) supplied by Caliper Lifesciences. In these heat maps, <50% inhibition is assigned as completely green and >95% inhibition is assigned as completely red.

deeply characterized. In vitro properties and in vivo rat pharmacokinetics (PK) for compounds **3f**, **3h**, and **3q** are shown in Table 4. Tertiary alcohol **3f** was an early example with good in vitro properties translating to reasonable in vivo rat

exposures, indicating that the core 3-amido pyrrolopyrazine is a drug-like scaffold and encouraging further optimization. Nitrile **3h** and bis-amide **3q** were designed and synthesized later in the optimization exercise and were two of our best examples with

Table 3. Cellular and HWB Potencies for Select Compounds^a

compd	PBMC (IL-2) IC ₅₀ (μM) ^b	PBMC (GM-CSF) IC ₅₀ (μM) ^b	PBMC (IFN-γ) IC ₅₀ (μM) ^b	HWB (IL-2) IC ₅₀ (μM) ^b
3e	0.211 ± 0.069	5.48 ± 0.96	3.38 ± 0.47	2.46 ± 0.34
3f	2.23 ± 0.56	>30	13.2 ± 0.3	15.7 ± 2.9
3h	0.214 ± 0.081	1.42 ± 0.33	2.57 ± 0.47	1.09 ± 0.29
3n	0.553 ± 0.048	2.03 ± 0.32	2.26 ± 0.084	5.02 ± 0.005
3p	0.328 ± 0.054	8.90 ± 2.16	2.54 ± 0.15	0.805 ± 0.241
3q	0.031 ± 0.003	0.188 ± 0.059	0.291 ± 0.079	1.008 ± 0.125
3r	0.030 ± 0.002	0.206 ± 0.022	0.141 ± 0.015	0.511 ± 0.047
3t	0.028 ± 0.002	0.321 ± 0.104	0.102 ± 0.011	1.15 ± 0.27
1	0.028 ± 0.001	0.184 ± 0.019	0.170 ± 0.012	0.054 ± 0.003

^aInhibition of phosphorylation of STAT5a or STAT1 in PBMCs or HWB. The IL-2 readouts are gated to CD3-expressing T-cells; the GM-CSF and IFN-γ readouts are gated to CD14-expressing monocytes. ^bMean ± SEM (standard error of the mean), $n \geq 3$ except for 3n HWB value ($n = 2$).

Table 4. In Vitro and in Vivo Properties of Select Compounds

in vitro						
compd	solubility ^a (μg/mL)	Caco ^b AB/BA	protein binding ^c (% free)	microsomal stability ^{d,f}		
3f	55.7	11.3/16.4	11.6	Cl _{int} (human) 32.0	Cl _{int} (rat) 38.2	
3h	<1	17.8/15.3	6.6	Cl _{int} (human) 27.7	Cl _{int} (rat) 50.3	
3q	32.7	2.1/24.6	3.4	Cl _{int} (human) 40.1	Cl _{int} (rat) 51.5	
in vivo rat (Hanover–Wistar) ^{e,f}						
compd	t _{1/2} (h)	Vd _{ss} (mL/kg)	Cl (mL/kg min)	% F	AUC (ng·h/mL)	C _{max} (ng/mL)
3f	4.4	1010	7.4	24	1090	429
0.5 mg/kg IV 2 mg/kg PO						
3h	0.66	1221	26.1	33	506	200
0.5 mg/kg IV 2 mg/kg PO						
3q	3.8	1063	14.6	25	1195	398
1 mg/kg IV 5 mg/kg PO						

^aLYSA (Lyophilized solubility assay). ^bPermeability in measured Caco-2 cells AB (apical to basolateral) and BA (basolateral to apical) movement of 10 μM test compound (50 μM test compound for 3q) in 7 days cultured Caco-2 cells (cm/s × 10⁻⁶), pH 7.4 on both sides. ^cEquilibrium dialysis, male and female human plasma. ^dLiver microsomal intrinsic clearance (μL/min/mg protein). ^eDoses were IV (intravenous) and PO (per os); mean values of 2–3 rats per sample time. ^fC_{max}, AUC and % F were determined after the oral dose and Cl, Vd_{ss} and t_{1/2} were determined from the IV dose.

Table 5. Further Cellular Profiling of 3q, 3t, and 1^a

	PBMC (IL-2) IC ₅₀ (μM) ^b	PBMC (GM-CSF) IC ₅₀ (μM) ^b	PBMC (IFN-γ) IC ₅₀ (μM) ^b	PBMC (IL-6) IC ₅₀ (μM) ^b (CD3)	PBMC (IL-6) IC ₅₀ (μM) ^b (CD14)
3q	0.031 ± 0.003	0.188 ± 0.059	0.291 ± 0.079	1.2 ± 0.6	0.864 ± 0.206 ^c
3t	0.028 ± 0.002	0.321 ± 0.104	0.102 ± 0.011	0.255 ± 0.135 ^c	0.175 ± 0.065 ^c
1	0.028 ± 0.001	0.184 ± 0.019	0.170 ± 0.012	0.38 ± 0.20	0.238 ± 0.07 ^c

^aInhibition of phosphorylation of STAT5a, STAT1, or STAT3 in PBMCs. The IL-2 readouts are gated to CD3-expressing T-cells; the GM-CSF and IFN-γ readouts are gated to CD14-expressing monocytes. The IL-6 readouts are gated to either CD3-expressing T-cells or to CD14-expressing monocytes, as noted. ^bMean ± SEM (standard error of the mean), $n \geq 3$ except for the IL-6 PBMC data noted with footnote c. ^c $n = 2$ data.

respect to the balance of properties with high enzyme and cellular potencies as well as kinase selectivities. Nitrile 3h had poor solubility, and bis-amide 3q had lower permeability and higher efflux in our Caco-2 assay (a common issue for the bis-amides); however, both compounds showed oral bioavailability in rat. Compound 3q was chosen for further study, as its superior solubility was likely to be more conducive to increasing exposures with higher doses in in vivo experiments.

Further Functional Characterization of Compound 3q. As described above, compound 3q was highly potent in both our JAK3 enzyme and IL-2 stimulated cellular assays, showed

selectivity for inhibition of JAK3 versus JAK1, had one of the cleanest Caliper selectivity profiles tested for this series, and appeared suitable for in vivo studies. We chose this compound for further characterization, including expanded kinase selectivity profiling. Compound 3q was sent to Kinomescan to test for compound binding against their entire kinase panel. The Kinomescan platform measures percent displacement of bait ligands by test compound. At 1 μM test compound concentration, compound 3q displaces >90% of ligand for only 41 out of 385 wild-type kinases tested (profiling data is included in the Supporting Information). Kinomescan also determined

K_d s for **3q** against the kinase domains of JAK3 (K_d 0.12 nM), JAK2 (K_d 0.18 nM), JAK1 (K_d 12 nM), and Tyk2 (K_d 16 nM). In these assays, compound **3q** shows very strong binding to JAK3 (and JAK2), with high selectivity (100x) against both JAK1 and Tyk2.

We expanded our human PBMC assays panels for compounds **3q**, **3t**, and Tofacitinib **1** (Table 5). We added two variations stimulating with IL-6, examining STAT3 phosphorylation in T-cells and monocytes, which is known to depend on JAK1, JAK2, and Tyk2. Notably, compound **3q** showed a 40-fold selectivity for inhibition of the IL-2 readout versus the IL-6 readout in T-cells and a 30-fold selectivity for inhibition versus the IL-6 readout in monocytes. Compounds **3t** and Tofacitinib **1** also showed selectivity for inhibition of the IL-2 readout but to a lesser degree against IL-6 for either readout. Our conclusion is that increased functional selectivity to inhibit IL-2 signaling versus IL-6 signaling is possible with increased enzyme-level selectivity to inhibit JAK3 versus JAK1.

We also examined the functional effects of compound **3q** on human T-cell response. Compound **3q** inhibits the proliferation of human CD4 and CD8 T cells in a dose-dependent manner upon stimulation by anti-CD3/anti-CD28 antibody-coated beads partially mimicking the activation signals brought to a T-cell by an antigen-presenting cell (see Supporting Information for details). Thus, compound **3q** is active in both mechanistic and functional cell-based assays using T-cells, one of the major cell types in which JAK3 is potentially relevant.¹²

Finally, an acute pharmacokinetic/pharmacodynamic (PK/PD) mouse model was developed to measure the inhibition of JAK family dependent signaling in vivo. As a bridging study between this model and our human cellular assays, we first evaluated compound **3q** in mouse whole blood (MWB) assays (Table 6). Compound **3q** potentially inhibits IL-2 stimulated

Table 6. Mouse Whole Blood (MWB) Potencies for Selected Compounds^a

	MWB (IL-2) IC ₅₀ (μM) ^b	MWB (GM-CSF) IC ₅₀ (μM) ^b	MWB (IFN-γ) IC ₅₀ (μM) ^b	MWB (IL-6) IC ₅₀ (μM) ^b
3q	0.18 (0.02)	1.1 (0.24)	0.17 (0.03)	9.9 (1.0)
3t	0.14 (0.02)	0.85 (0.09)	0.11 (0.01)	2.01 (0.16)
1	0.05 (0.01)	2.04 (0.39)	0.18 (0.04)	1.72 (0.11)

^aInhibition of phosphorylation of STAT5a, STAT1 or STAT3 in MWB. ^bMean (SEM (standard error of the mean)), $n \geq 4$.

STAT5 phosphorylation in mouse whole blood (MWB), with selectivity against GM-CSF and IL-6 stimulated readouts, as observed in human PBMCs. In our MWB assays, compound **3q** did not show selectivity for inhibiting the IL-2 readout versus the IFN-γ readout, suggesting a potential for species difference of IFN-γ signaling in human and mouse systems. For comparison purposes, we also evaluated compound **3t** and Tofacitinib **1** in the MWB assays. All three compounds showed selectivity for inhibition of the IL-2 assay vs the IL-6 assay, with the rank order of selectivity corresponding to the rank order of selectivity for JAK3 versus JAK1 (i.e., **3q** is more selective than **1** and **3t**).

In the acute PK/PD mouse model, animals were orally treated with different doses of compound **3q** (0.3 to 100 mg/kg) and whole blood was collected 2 h later, ex vivo stimulated with IL-2, GM-CSF, or IL-6, and the appropriate STAT phosphorylation was measured by flow cytometry. Figure 6 shows response versus dose curves for the three different stimulations plus the measured

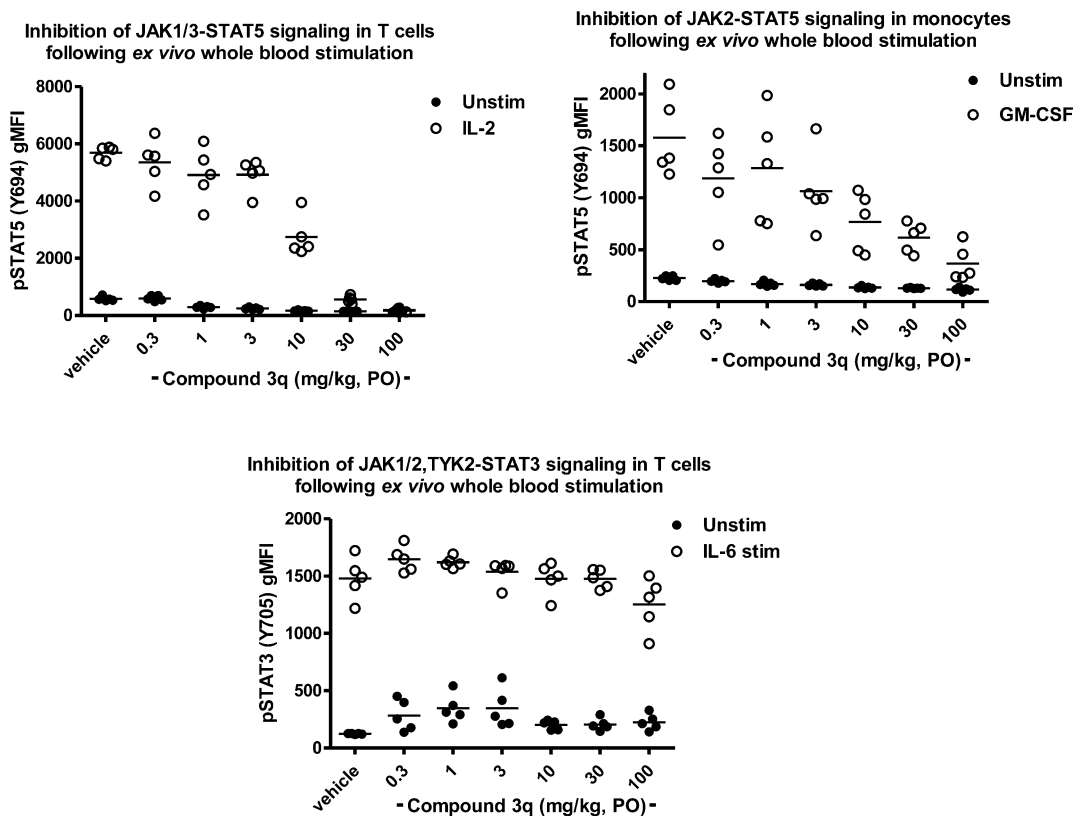
plasma concentrations of **3q** for each dose. Compound **3q** prevented IL-2-driven STAT5 phosphorylation in a dose- and concentration-dependent manner, with approximately 50% inhibition observed at the 10 mg/kg dose (plasma concentration ~480 nM). Complete inhibition of IL-2-driven STAT5 phosphorylation was achieved at the 30 mg/kg dose (plasma concentration ~2087 nM). Compound **3q** also inhibited GM-CSF-driven STAT5 phosphorylation in a dose- and concentration-dependent manner, but a complete inhibition of STAT5 phosphorylation in blood monocytes was not achieved with the maximum dose tested of 100 mg/kg (plasma concentration ~6597 nM). Lastly, when whole blood from mice treated with compound **3q** was stimulated with IL-6 ex vivo, only 15% inhibition was observed of IL-6-driven pSTAT3 phosphorylation at the maximum tested dose of 100 mg/kg. Thus, the PK/PD results clearly show that target engagement can be achieved after oral administration of compound **3q** and that compound **3q** is JAK3 selective in vivo, as judged by higher potency inhibiting JAK1/JAK3- vs JAK2- or JAK1/JAK2/TYK2-driven signaling in whole blood assays.

Discussion and Exploratory siRNA Studies. We were able to optimize a new chemical series, 3-amidopyrrolopyrazines, into highly potent JAK inhibitors with reasonable kinome selectivity profiles. Structurally related examples with similar potencies against JAK3 but differing potencies against JAK1 show similar cellular potencies in an IL-2 induced STAT5 phosphorylation assay. Our results suggest that JAK3 plays an essential role in IL-2 induced STAT5 phosphorylation. At first glance, this conclusion appears to contradict that reached by the Novartis group, which showed that selective depletion of JAK1 by siRNA in T-cells is more detrimental to IL-2 signaling than depletion of JAK3.¹⁹ We found similar results in our own siRNA work (see below).

Novartis also published their own JAK3-selective compound, which shows poor activity in a similar IL-2 dependent cellular assay. Novartis's JAK3-selective compound is significantly more selective than compound **3q** against JAK1 at the enzyme level (based on comparison with Tofacitinib as control) and, unlike compound **3q**, also shows high selectivity against JAK2. The compound published by the Pharmacopeia group, with which they concluded that JAK1 inhibition is not required for potent inhibition of IL-2 signaling, has enzyme selectivities similar to compound **3q**. These observations suggest at least two possible explanations for compound **3q**'s retained potency for inhibiting IL-2 signaling. One possibility is that **3q**'s level of selectivity against JAK1 is simply not high enough to have a strong differential effect in this particular cellular context. A second possibility is that JAK2 may also play a role in IL-2 signaling.²⁷

We performed siRNA knockdown studies on JAK3, JAK2, and JAK1 in primary T-cells, looking for effects on IL-2 induced STAT5 phosphorylation (Figure 7). Our findings for JAK1 (strong involvement in STAT5 phosphorylation) and JAK3 (weaker involvement in STAT5 phosphorylation) qualitatively agree with the findings of the Novartis group. The Novartis group did not include JAK2 in their published studies; in our work, we found no effect of JAK2 depletion on IL-2 induced STAT5 phosphorylation at the siRNA concentrations tested. Thus, inhibition of JAK2 by compound **3q** is unlikely to be the driver for activity in our IL-2 cellular assays.

We cannot discount the possibility that the diminished JAK1 inhibitory activity of compound **3q** remains a significant driver of potency against IL-2 signaling. However, our results do confirm that improved selectivity for IL-2 signaling over IL-6 signaling, with retention of IL-2 cellular potency, is achievable for JAK3



PO Dose (mg/kg)	0.3	1	3	10	30	100
[ng/mL]	7.4 ± 2	30.7 ± 7	51.8 ± 17	183 ± 55	794 ± 117	2510 ± 475
[nM]	~20	~81	~136	~480	~2087	~6597

Figure 6. Inhibition of STAT phosphorylation in mice treated with compound **3q** in an acute PK/PD model.

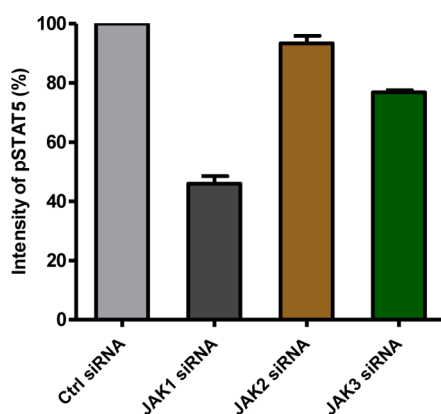


Figure 7. siRNA depletion studies on JAK1–3 in primary T-cells. Human primary T cells were transfected with siRNAs targeting JAK1, JAK2, JAK3, or scramble siRNA (Ctrl RNA) by Amaxa electroporation, and IL-2 induced phosphorylation of STAT5 was determined by flow cytometric analysis. The intensity of pSTAT5 (%) was normalized to control scramble siRNA treatment group represented as percentage (%). The experiment was repeated in three independent experiments on three different donors. Gene knockdown confirmation studies are included in the Supporting Information.

inhibitors with improved selectivity against JAK1. Importantly, the cellular potencies and selectivities for our most highly optimized compound **3q** was translated to in vivo potency and selectivity in an acute PK/PD mouse model. Compound **3q** may therefore be an excellent tool compound for further dissecting the roles of these different pathways in other in vivo models.

EXPERIMENTAL SECTION

Chemistry. Reagents and solvents were obtained from commercial suppliers and were used without further purification. ^1H NMR measurements were recorded at 300 MHz using a Bruker AMX 300 instrument. Chromatographic purifications were performed with automated chromatography systems using prepacked silica gel cartridges supplied by Thomson Instrumental Co. or by TeleDyne Isco Inc. Melting points recorded were uncorrected. Purity and characterization of compounds were established by a variety of elemental analysis, LC/MS, and NMR analytical techniques, and purities were >95% for all final products.

2-Bromo-5-(2-trimethylsilyanyl-ethoxymethyl)-5H-pyrrolo[2,3-*b*]pyrazine-7-carbaldehyde (4). To a partial suspension of 2-bromo-5H-pyrrolo[2,3-*b*]pyrazine (5.0 g, 25 mmol) in 100 mL of 1,4-dioxane was added 2 M aqueous sodium hydroxide solution (25 mL, 50 mmol) and 37% aqueous formaldehyde solution (19 mL, 250 mmol). The dark homogeneous reaction mixture was stirred at 25 °C for 16 h, and then the organic solvent was removed under reduced pressure. The

aqueous residue was adjusted to pH 7 with 1 M aqueous hydrochloric acid and then extracted twice with ethyl acetate. The combined organic phases were concentrated to afford 2.60 g of (2-bromo-5-hydroxymethyl-pyrrolo[2,3-*b*]pyrazin-7-yl)-methanol as an orange solid. Upon standing, a thick brown precipitate formed in the aqueous phase. The precipitate was collected by filtration and dried. The brown solid was extracted with three 200 mL portions of hot 10% methanol/ethyl acetate. The extracts were combined and evaporated to provide an additional 3.05 g of (2-bromo-5-hydroxymethyl-pyrrolo[2,3-*b*]pyrazin-7-yl)-methanol as an orange solid. The overall yield was 5.65 g (87%) of crude (2-bromo-5-hydroxymethyl-pyrrolo[2,3-*b*]pyrazin-7-yl)-methanol, which was carried directly to the next step. ¹H NMR (300 MHz, DMSO-*d*₆) δ ppm 8.42 (s, 1 H), 7.97 (s, 1 H), 6.91 (br s, 1 H), 5.59 (br s, 2 H), 5.13 (br s, 1 H), 4.65 (br s, 2 H). MS (EI/CI) *m/z*: 258, 260 (M + H).

To a suspension of the above-prepared (2-bromo-5-hydroxymethyl-pyrrolo[2,3-*b*]pyrazin-7-yl)-methanol (5.65 g, 21.9 mmol) in 150 mL of tetrahydrofuran was added a solution of 2 M aqueous sodium hydroxide solution (33 mL, 66 mmol). The mixture was stirred for 16 h, and then the organic layer was removed under reduced pressure. The aqueous residue was adjusted to pH 4 with 1 M aqueous hydrochloric acid. The resulting precipitate was collected via filtration and rinsed with water to afford 3.68 g of (2-bromo-5H-pyrrolo[2,3-*b*]pyrazin-7-yl)-methanol as a yellow solid. The filtrate was extracted twice with ethyl acetate, and the combined organic phases were concentrated under reduced pressure to provide an additional 0.92 g of (2-bromo-5H-pyrrolo[2,3-*b*]pyrazin-7-yl)-methanol as a yellow solid. The overall yield was 4.60 g (92%) of crude (2-bromo-5H-pyrrolo[2,3-*b*]pyrazin-7-yl)-methanol, which was carried directly to the next step. ¹H NMR (300 MHz, DMSO-*d*₆) δ ppm 12.20 (br s, 1 H), 8.35 (s, 1 H), 7.87 (s, 1 H), 4.98 (t, *J* = 5.3 Hz, 1 H), 4.63 (d, *J* = 4.9 Hz, 2 H). MS (EI/CI) *m/z*: 228, 230 (M + H).

A stock solution of Jones reagent (2.67 M) was prepared by carefully adding concentrated sulfuric acid (2.3 mL) to chromium trioxide (2.67 g) and then diluting with water to a final volume of 10 mL. To a partial suspension of the above-prepared (2-bromo-5H-pyrrolo[2,3-*b*]pyrazin-7-yl)-methanol (4.60 g, 20.1 mmol) in 300 mL of acetone was slowly added the Jones reagent (9.0 mL, 24 mmol). During the addition, the starting material gradually dissolved and a thick green precipitate formed. The reaction mixture was stirred for 15 min and then quenched with 2 mL of 2-propanol and filtered through Celite 545, rinsing with acetone. The filtrate was concentrated to provide 4.76 g ("104%") of crude 2-bromo-5H-pyrrolo[2,3-*b*]pyrazine-7-carbaldehyde as a yellow-orange solid, which was carried directly to the next step. ¹H NMR (300 MHz, DMSO-*d*₆) δ ppm 13.36 (br s, 1 H), 10.04 (s, 1 H), 8.80 (s, 1 H), 8.55 (s, 1 H). MS (EI/CI) *m/z*: 226, 228 (M + H).

To a solution of the above-prepared crude 2-bromo-5H-pyrrolo[2,3-*b*]pyrazine-7-carbaldehyde (4.7 g) in 50 mL of *N,N*-dimethylformamide at 0 °C was added sodium hydride (60% in mineral oil, 1.2 g, 30 mmol). The reaction mixture was stirred at 25 °C for 30 min and then cooled to 0 °C. The mixture was then treated with 2-(trimethylsilyl)ethoxymethyl chloride (4.3 mL, 24 mmol). The reaction mixture was allowed to warm to 25 °C, stirred for 1 h, and then quenched with water and extracted three times with ethyl acetate. The combined organics were sequentially washed with three portions of water and a saturated aqueous sodium chloride solution and then dried over magnesium sulfate, filtered, and concentrated. The residue was purified by silica gel chromatography (20–30% ethyl acetate/hexanes) to afford 3.82 g (51%; 42% over four steps) of 2-bromo-5-(2-trimethylsilyl-ethoxymethyl)-5H-pyrrolo[2,3-*b*]pyrazine-7-carbaldehyde (4) as a yellow solid. ¹H NMR (300 MHz, DMSO-*d*₆) δ ppm 10.07 (d, *J* = 0.8 Hz, 1 H), 8.97 (s, 1 H), 8.65 (s, 1 H), 5.71 (s, 2 H), 3.53–3.61 (m, 2 H), 0.79–0.88 (m, 2 H), –0.09 (s, 9 H). MS (EI/CI) *m/z*: 356, 358 (M + H).

2-Cyclopropyl-5-(2-trimethylsilyl-ethoxymethyl)-5H-pyrrolo[2,3-*b*]pyrazine-7-carbaldehyde (5). A mixture of 2-bromo-5-(2-trimethylsilyl-ethoxymethyl)-5H-pyrrolo[2,3-*b*]pyrazine-7-carbaldehyde (0.330 g, 0.930 mmol), cyclopropylboronic acid (0.120 g, 1.40 mmol), tricyclohexylphosphine (0.026 g, 0.09 mmol), palladium(II) acetate (0.010 g, 0.046 mmol), potassium phosphate tribasic (0.630 g, 2.97 mmol), 4 mL of toluene, and 0.5 mL of water was flushed with argon for 5 min. The reaction mixture was stirred at 100 °C for 18 h and

then allowed to cool and filtered through a pad of Celite 545, rinsing with ethyl acetate. The filtrate was concentrated under reduced pressure, and the residue was purified by silica gel chromatography (10% ethyl acetate/hexanes) to afford 0.240 g (81%) of 2-cyclopropyl-5-(2-trimethylsilyl-ethoxymethyl)-5H-pyrrolo[2,3-*b*]pyrazine-7-carbaldehyde (5) as a yellow powder. ¹H NMR (300 MHz, CDCl₃) δ ppm 10.38 (s, 1 H), 8.26 (s, 1 H), 8.22 (s, 1 H), 5.68 (s, 2 H), 3.53–3.61 (m, 2 H), 2.26–2.36 (m, 1 H), 1.09–1.24 (m, 4 H), 0.89–0.97 (m, 2 H), –0.04 (s, 9 H). MS (EI/CI) *m/z* 318 (M + H).

2-Cyclopropyl-5-(2-trimethylsilyl-ethoxymethyl)-5H-pyrrolo[2,3-*b*]pyrazine-7-carboxylic Acid (6). To a mixture of 2-cyclopropyl-5-(2-trimethylsilyl-ethoxymethyl)-5H-pyrrolo[2,3-*b*]pyrazine-7-carbaldehyde (0.24 g, 0.75 mmol) in 10 mL of 1,4-dioxane and 2 mL of water at 0 °C was added sulfamic acid (0.44 g, 4.5 mmol) and then dropwise a solution of 80% sodium chlorite (0.09 g, 0.8 mmol) and potassium dihydrogen phosphate (1.22 g, 9.00 mmol) in 6 mL of water. The reaction mixture was allowed to warm to 25 °C and stirred for 2 h and then partitioned between water and ethyl acetate. The organic phase was washed with a saturated aqueous sodium chloride solution, dried over sodium sulfate, filtered, and concentrated under reduced pressure. The residue was triturated with hexanes to obtain 0.22 g (87%) of 2-cyclopropyl-5-(2-trimethylsilyl-ethoxymethyl)-5H-pyrrolo[2,3-*b*]pyrazine-7-carboxylic acid as a light-yellow powder (6). ¹H NMR (300 MHz, CDCl₃) δ ppm 8.37 (s, 1 H), 8.28 (s, 1 H), 5.65–5.70 (m, 2 H), 3.52–3.63 (m, 2 H), 2.20–2.32 (m, 1 H), 1.13–1.22 (m, 4 H), 0.88–0.98 (m, 2 H), –0.03 (s, 9 H). MS (EI/CI) *m/z* 334 (M + H).

2-Cyclopropyl-5H-pyrrolo[2,3-*b*]pyrazine-7-carboxylic Acid [(*R*)-1-(3-Cyano-azetidine-1-carbonyl)-2,2-dimethyl-propyl]-amide (3q). A solution of [(*R*)-1-(3-cyano-azetidine-1-carbonyl)-2,2-dimethyl-propyl]-carbamic acid *tert*-butyl ester (see preparation below) (0.093 g, 0.32 mmol) in 3 mL of dichloromethane at 0–5 °C was treated with 1 mL of trifluoroacetic acid. The reaction solution was allowed to warm to 25 °C and stirred for 3 h and then concentrated to afford crude (*R*)-1-(3-cyano-azetidine-1-carbonyl)-2,2-dimethyl-propyl-ammonium trifluoroacetate as a colorless glass, which was used directly in the next step.

A solution of 2-cyclopropyl-5-(2-trimethylsilyl-ethoxymethyl)-5H-pyrrolo[2,3-*b*]pyrazine-7-carboxylic acid (0.070 g, 0.21 mmol) in 2 mL of acetonitrile was treated with *O*-(benzotriazol-1-yl)-*N,N,N',N'*-tetramethyluronium tetrafluoroborate (0.081 g, 0.25 mmol), the above-prepared crude (*R*)-1-(3-cyano-azetidine-1-carbonyl)-2,2-dimethyl-propyl-ammonium trifluoroacetate, and *N,N*-diisopropylethylamine (0.13 mL, 0.74 mmol). The reaction mixture was stirred at 25 °C for 16 h and then was diluted with water and extracted with ethyl acetate. The organic phase was washed with a saturated aqueous sodium chloride solution, dried over sodium sulfate, filtered, and concentrated. The residue was purified by silica gel chromatography (0–5% methanol/dichloromethane) to afford 0.092 g (85%) of 2-cyclopropyl-5-(2-trimethylsilyl-ethoxymethyl)-5H-pyrrolo[2,3-*b*]pyrazine-7-carboxylic acid [(*R*)-1-(3-cyano-azetidine-1-carbonyl)-2,2-dimethyl-propyl]-amide as a colorless semisolid. ¹H NMR (300 MHz, CDCl₃) δ ppm 8.93 (d, *J* = 9.1 Hz, 1 H), 8.30 (s, 1 H), 8.17 (s, 1 H), 5.59–5.68 (m, 2 H), 4.74–4.97 (m, 1 H), 4.16–4.58 (m, 4 H), 3.45–3.58 (m, 3 H), 2.16–2.26 (m, 1 H), 1.32–1.41 (m, 1 H), 1.07–1.20 (m, 12 H), 0.86–0.95 (m, 2 H), –0.09 to –0.02 (m, 9 H). MS (EI/CI) *m/z* 511 (M + H).

A solution of the above-prepared 2-cyclopropyl-5-(2-trimethylsilyl-ethoxymethyl)-5H-pyrrolo[2,3-*b*]pyrazine-7-carboxylic acid [(*R*)-1-(3-cyano-azetidine-1-carbonyl)-2,2-dimethyl-propyl]-amide (0.092 g, 0.18 mmol) in 2 mL of dichloromethane was treated with 0.6 mL of trifluoroacetic acid. The reaction solution was stirred at 25 °C for 2 h and was then neutralized by addition of a saturated aqueous sodium bicarbonate solution. The resultant mixture was extracted three times with ethyl acetate, and the combined organic phases were washed with saturated sodium chloride solution, dried over sodium sulfate, filtered, and concentrated. The residue was redissolved in 8 mL of ethanol, and the resulting solution was treated with sodium acetate (0.30 g, 3.6 mmol). The mixture was stirred at 50 °C for 20 h, allowed to cool, and then treated with water and ethyl acetate. Layers were separated, the aqueous phase was extracted twice with ethyl acetate, and the combined

organic layers were washed with a saturated aqueous sodium chloride solution, dried over sodium sulfate, filtered, and concentrated. The residue was purified by silica gel chromatography (0–5% methanol/dichloromethane) to afford 0.052 g (75%) of 2-cyclopropyl-5H-pyrrolo[2,3-*b*]pyrazine-7-carboxylic acid [(*R*)-1-(3-cyano-azetidine-1-carbonyl)-2,2-dimethyl-propyl]-amide as an off-white solid; mp 181–183 °C. ¹H NMR (300 MHz, DMSO-*d*₆) δ ppm 12.63 (br s, 1 H), 8.63–8.73 (m, 1 H), 8.40–8.44 (m, 1 H), 8.26–8.34 (m, 1 H), 4.41–4.68 (m, 2 H), 4.26–4.36 (m, 1 H), 3.98–4.24 (m, 2 H), 3.74–3.91 (m, 1 H), 2.26–2.39 (m, 1 H), 1.14–1.26 (m, 1 H), 1.04 (s, 11 H), 0.92–0.99 (m, 1 H). MS (EI/CI) *m/z* 381 (M + H). Analysis Calculated for C₂₀H₂₄N₆O₂·(0.16H₂O): C, 62.67; H, 6.39; N, 21.92. Found: C, 62.65; H, 6.39; N, 21.63. [α]_D²⁸ (c = 0.5, methanol) –149.6 °.

[(*R*)-1-(3-Cyano-azetidine-1-carbonyl)-2,2-dimethyl-propyl]-carbamic Acid *tert*-Butyl Ester. A solution of *N-tert*-butoxycarbonyl-*D-tert*-leucine (0.500 g, 2.16 mmol), *O*-(benzotriazol-1-yl)-*N,N,N',N'*-tetramethyluronium tetrafluoroborate (0.83 g, 2.6 mmol), and 3-cyanoazetidinium chloride (0.270 g, 2.28 mmol) in 22 mL of dichloromethane was treated with *N,N*-diisopropylethylamine (0.94 mL, 5.4 mmol), and the reaction mixture was stirred at 25 °C for 16 h. The mixture was then treated with water and extracted twice with ethyl acetate. The combined organic layers were washed with a saturated aqueous sodium chloride solution, dried over sodium sulfate, filtered, and concentrated. The residue was purified by silica gel chromatography (20% ethyl acetate/hexanes) to afford 0.39 g (61%) of [(*R*)-1-(3-cyano-azetidine-1-carbonyl)-2,2-dimethyl-propyl]-carbamic acid *tert*-butyl ester as a white solid. ¹H NMR (300 MHz, DMSO-*d*₆) δ ppm 6.75–6.89 (m, 1 H), 4.28–4.57 (m, 2 H), 3.93–4.21 (m, 2 H), 3.67–3.88 (m, 2 H), 1.31–1.45 (m, 9 H), 0.91 (d, *J* = 3.3 Hz, 9 H). MS (EI/CI) *m/z* 318 (M + Na).

Biological Methods. JAK1–3 Kinase Inhibition. The ability of compounds to inhibit Janus kinase enzymes 1, 2, or 3 was determined by a kinase filtration assay. JAK1 was purchased from Invitrogen and JAK2 and 3 proteins were prepared in house. Briefly, 6 nM JAK1 (866–1154 amino acids), 1 nM JAK2 (JAK2-SF21c 828–1132), or 0.1 nM of JAK3 enzyme (810–1124 amino acids) were preincubated with compound at room temperature for 10 min in 50 mM HEPES buffer and 10 mM magnesium chloride (MgCl₂) that was supplemented with 1 mM dithiothreitol (DTT) and 1 mg/mL bovine serum albumin (BSA). The kinase reactions for all of the enzymes were initiated by the addition of a substrate cocktail that contained 1.5 μM adenosine triphosphate (ATP), 0.025 μCi ATP-γ-P³³, and 0.2 mM of biotinylated synthetic peptide (Biomer Technology: Biotin-KALETDKKEYTVKD) at a final volume of 40 μL. The reaction was carried out at room temperature for 30 min for JAK2 and JAK3, and for 1 h for JAK1. Reactions were quenched by transferring 25 μL to a filter plate (Millipore MABVN0B50, 1.2 μM pore size) containing 100 μL of prepared 10% streptavidin beads in 1× PBS (Mg and Ca²⁺ free) and 100 mM ethylene diamine tetra-acetic acid (EDTA). The bead/terminated solution was mixed and incubated for 30 min at room temperature. Using a vacuum manifold, plates were washed three times with 240 μL of 2 M aqueous sodium chloride solution, three times with 2 M aqueous sodium chloride +1% phosphoric acid solution, and twice with water. The plates were then dried in a 60 °C oven for 1 h. Finally, 70 μL of Microscint-20 was added and sealed. Resulting P³³ incorporation was determined by counting the plate in a Packard TopCount.

Inhibition of STAT Phosphorylation in Peripheral Blood Mononuclear Cells (PBMCs) or Human Whole Blood (HWB). PBMCs or HWB isolated from healthy volunteers were incubated with compounds for 30 min at 37 °C. The PBMCs or HWB were then treated with either 100 ng/mL IL-2 or 20 pg/mL GM-CSF or 100 ng/mL IFNγ or 100 ng/mL IL-6, and the PBMCs or HWB were incubated for an additional 20 min at 37 °C. PBMCs or HWB were lysed and/or fixed and permeabilized (perm buffer III, BD Bioscience) and then stained with anti-CD3 FITC and anti-CD14 PE and either anti-pSTAT5 or anti-pSTAT1 or anti-pSTAT3. Flow cytometry analysis was performed using an LSRII instrument (BD Bioscience). Data analysis was done using Flowjo software. IC₅₀ values were generated using ActivityBase software.

Experimental Animals. All procedures using animals and in vivo procedures were approved by Roche's Institutional Animal Care and

Use Committee (IACUC), and performed according to guidelines established by the Guide for the Care and Use of Laboratory Animals by National Research Council and by Association for the Assessment and Accreditation of Laboratory Animal Care International (AAALAC), and American Veterinary Medical Association Guidelines on Euthanasia (2007). Animals used for the present studies were adult female C57BL/6 mice (Jackson Laboratory, Bar Harbor, Maine) and female Wistar/Han rats (Charles River, Hollister, CA).

Inhibition of STAT Phosphorylation in Mouse Whole Blood (MWB). Whole blood from healthy C57BL/6 mice (*n* = 20) was collected in heparinized tubes and pooled then incubated with compound 3q at different concentrations (0.003 μM to 100 μM) for 30 min at 37 °C. Blood cells were stimulated for 20 min at 37 °C with recombinant mouse IL-2, GM-CSF or IL-6 (eBioscience) at EC90 concentration, which was previously determined using that respective cytokine batch. Red blood cells were then lysed with 1X Lyse/Fix solution (BD Bioscience) for 20 min at room temperature. Cells were pelleted, resuspended in Phosflow Perm Buffer III (BD Bioscience), and left on ice for 30 min. Cells were washed twice using 1X Perm/Wash buffer then resuspended in a volume of 100 μL prior to staining with fluorochrome-conjugated antimouse antibodies (BD Bioscience): staining A = anti-TCRβ PE, anti-CD4 FITC, anti-CD25 PerCP-Cy5.5, and anti-pSTAT5 AF647; staining B = anti-CD11b FITC, anti-TCRβ PE, anti-B220 PerCP-Cy5, and anti-pSTAT5 AF647; staining C = anti-CD11b FITC, anti-TCRβ PE, anti-B220 PerCP-Cy5, and anti-pSTAT3 AF647. Flow cytometry sample acquisition and data analysis were performed using an LSRII instrument and Flowjo software, respectively. IC₅₀ values were generated using ActivityBase software.

Microsomal Stability. Microsome preparations prepared from male and female rat or human livers were obtained from BD Biosciences (Woburn, MA). Test compounds were diluted from 10 mM stock solutions in DMSO; incubations contained <1% residual DMSO. Incubations were performed in 96-well deep-well plates with a final incubation volume of 600 μL. Incubations contained 1–2 μM test compound, 0.5 mg/mL liver microsomes, and NADPH regenerating system. Aliquots of 50 μL were removed at time points from 1 to 45 min, quenched in acetonitrile containing internal standard, and cooled prior to centrifugation and analysis by LC-MS/MS. The natural log of the ratio of the test compound peak area to the internal standard peak area was plotted against incubation time, and the slope of a linear fit of the initial rate of compound disappearance was used to calculate the intrinsic clearance.

$$Cl_{int} (\mu\text{L}/\text{min}/\text{mg}) = -\text{slope} (\text{min}^{-1}) \times 1000 \\ / [\text{protein concentration} (\text{mg}/\text{mL})]$$

Pharmacokinetics. Male Wistar/Han (CRL:WI) rats (Charles River Laboratories, Hollister, CA or Raleigh, NC) used in these studies weighed between 180 and 300 g and were surgically implanted with cannulas in the jugular and/or femoral veins. All studies were conducted under IACUC approved protocols, and animals were allowed free access to food and water. Single intravenous bolus doses were administered into the tail vein or into the jugular cannula of dual-cannulated animals; the remaining cannulas were used for blood collection. Single oral doses were administered by gavage. Blood was collected into tubes containing EDTA at typically 0.08 (IV only), 0.25, 0.5, 1, 2, 4, 6, 8, and 24 h after dosing. Plasma concentrations were determined by a liquid chromatography/tandem mass spectrometry method (LC/MS/MS) following protein precipitation with acetonitrile.

In Vivo Mouse PK/PD Model. Adult (10–12 weeks old) C57BL/6 mice were randomized into experimental groups (*n* = 5/group) including control vehicle group and compound 3q treated groups (0.3, 1, 3, 10, 30, and 100 mg/kg). According to their respective group, mice received a single oral suspension dose of compound 3q prepared in aqueous vehicle or vehicle alone containing 0.9% NaCl, 0.5% sodium carboxymethyl cellulose, 0.4% polysorbate 80, and 0.9% benzyl alcohol. Two hours after treatment by oral gavage, mice were euthanized with CO₂ asphyxiation for collecting whole blood in heparinized tubes. Whole blood from the respective mice was then ex vivo stimulated with IL-2, GM-CSF, or IL-6 at EC₉₀ concentration. The subsequent

experimental steps (from red blood cell lysis step to flow cytometry analysis) were similar to that used in the MWB assay, as previously described in this manuscript.

Human T Cell siRNA Transfection and Activation Assay. Primary human T cells were enriched from PBMC by using Pan T Cell Isolation Kit II (Miltenyi Biotec GmbH, Germany) and resuspended in PRMI-1640 culture medium supplemented with 10% FBS (Invitrogen, Carlsbad, CA). T cells were transfected with siRNAs targeting JAK1, JAK2, JAK3, or scramble control siRNA (Invitrogen) with Amaxa P3 Primary Cell 4D-Nucleofector X kit (Lonza Cologne GmbH, Germany) according to manufacturer's protocol using program "FI-115" in 4D-Nucleofector (Lonza). Transfected cells were transferred into 12-well plate and allowed 48 h of incubation at 37 °C followed by stimulation with IL2 (100 ng/mL, R&D Systems) for 20 min. Cells were fixed with 1.5% formaldehyde for 10 min at room temperature and then permeabilized with BD Phosflow Perm Buffer III at 4 °C overnight. Fixed and permeabilized cells were washed with FACS staining buffer (PBS with 2% FBS) twice, stained with FITC antihuman CD3 and Alexa Fluor 647 anti-STAT5 (pY694), and quantitated for pSTAT5 fluorescence intensity gated on CD3⁺ T cell population.

Protein Crystallography. JAK3 kinase domain (amino acids 811–1124, C1040S/C1048S) at 10–15 mg/mL in 50 mM HEPES (pH 8.0), 0.5 M NaCl, 20% glycerol, 5 mM DTT, 0.05% *n*-octyl- β -D-glucoside was incubated on ice for 1 h with 50 mM DTT, 0.75 mM inhibitor in DMSO, and 0.26% phenylurea (originally identified from Hampton Research Silver Bullet F10, later also described by others²⁴). For crystallization by vapor diffusion in hanging drops at 20 °C, 700 nL of JAK3–inhibitor complex solution was mixed with 300 nL of 24–34% PEG 3350, 0.1 M MES (pH 6.0), 0.2 M MgCl₂, and 150 nL of crystal seed solution. Crystals typically appeared overnight as rods or bipyramidal prisms. They were cryoprotected by gradually adding glycerol to 20% and flash-cooled in liquid nitrogen. Synchrotron data collection was provided by Reciprocal Space Consulting, LLC (Oakland, California) at beamline 9–2 of the Stanford Synchrotron Radiation Laboratory (Palo Alto, California) and beamline 5.0.2 of the Advanced Light Source (Berkeley, California) using ADSC Quantum 315 CCD detectors. The diffraction images were processed with DENZO, and the intensities were scaled with SCALEPACK.²⁸ The structure of the first JAK3–ligand complex was solved with the molecular replacement program PHASER²⁹ using the crystal structure of JAK3 kinase domain in complex with a staurosporine analogue³⁰ (PDB accession no. 1YVJ) as search model. The solution found was a JAK3 monomer in space group P2₁2₁2 with the unit cell dimensions $\alpha = 47$ Å, $\beta = 76$ Å and $\gamma = 90$ Å. The same crystal form has also been obtained for a similar JAK3 kinase domain variant.²⁴ The model was refined against the experimental data, and electron density maps were calculated using REFMAC5.³¹ Subsequent JAK3–ligand structures were determined by rigid body refinement. The structure models were built with the graphics software COOT.³²

■ ASSOCIATED CONTENT

● Supporting Information

Experimental procedures and analytical data for final compounds 3a–3p and 3r–3t, Kinomesan selectivity data for compound 3q, CD4 and CD8 cell proliferation studies, response versus plasma concentration curves for the mouse acute PK/PD model studies, and gene knockdown confirmation studies for the siRNA study. This material is available free of charge via the Internet at <http://pubs.acs.org>.

Accession Codes

Protein crystal structure coordinates and structure factors are deposited in the RCSB Protein Data Bank with the accession numbers 4HVD, 4HVG, 4HVH, and 4HVI.

■ AUTHOR INFORMATION

Corresponding Author

*Phone: 973-235-2717. Fax: 973-235-6263. E-mail: michael.soth@roche.com.

Notes

The authors declare no competing financial interest.

■ REFERENCES

- (1) Takeshita, T.; Asao, H.; Ohtani, K.; Ishii, N.; Kumaki, S.; Tanaka, N.; Munakata, H.; Nakamura, M.; Sugamura, K. Cloning of the γ chain of the human IL-2 receptor. *Science* **1992**, 257 (5068), 379–382.
- (2) Rochman, Y.; Spolski, R.; Leonard, W. J. New insights into the regulation of T cells by γ c family cytokines. *Nature Rev. Immunol.* **2009**, 9 (7), 480–490.
- (3) Macchi, P.; Villa, A.; Giliani, S.; Sacco, M. G.; Frattini, A.; Porta, F.; Ugazio, A. G.; Johnston, J. A.; Candotti, F.; O'Shea, J. J.; Vezzoni, P.; Notarangelo, L. D. Mutations of Jak-3 gene in patients with autosomal severe combined immune deficiency (SCID). *Nature* **1995**, 377 (6544), 65–68.
- (4) Russell, S. M.; Tayebi, N.; Nakajima, H.; Riedy, M. C.; Roberts, J. L.; Aman, M. J.; Migone, T. S.; Noguchi, M.; Markert, M. L.; Buckley, R. H.; O'Shea, J. J.; Leonard, W. J. Mutation of Jak3 in a patient with SCID: essential role of Jak3 in lymphoid development. *Science* **1995**, 270 (5237), 797–800.
- (5) Noguchi, M.; Yi, H.; Rosenblatt, H. M.; Filipovich, A. H.; Adelstein, S.; Modi, W. S.; McBride, O. W.; Leonard, W. J. Interleukin-2 receptor gamma chain mutation results in X-linked severe combined immunodeficiency in humans. *Cell* **1993**, 73 (1), 147–157.
- (6) Witthuhn, B. A.; Quelle, F. W.; Silvennoinen, O.; Yi, T.; Tang, B.; Miura, O.; Ihle, J. N. JAK2 associates with the erythropoietin receptor and is tyrosine phosphorylated and activated following stimulation with erythropoietin. *Cell* **1993**, 74 (2), 227–236.
- (7) Quelle, F. W.; Sato, N.; Witthuhn, B. A.; Inhorn, R. C.; Eder, M.; Miyajima, A.; Griffin, J. D.; Ihle, J. N. JAK2 associates with the beta c chain of the receptor for granulocyte-macrophage colony-stimulating factor, and its activation requires the membrane-proximal region. *Mol. Cell. Biol.* **1994**, 14 (7), 4335–4341.
- (8) Lütticken, C.; Wegenka, U. M.; Yuan, J.; Buschmann, J.; Schindler, C.; Ziemiecki, A.; Harpur, A. G.; Wilks, A. F.; Yasukawa, K.; Taga, T.; et al. Association of transcription factor APRF and protein kinase Jak1 with the interleukin-6 signal transducer gp130. *Science* **1994**, 263 (5143), 89–92.
- (9) Narazaki, M.; Witthuhn, B. A.; Yoshida, K.; Silvennoinen, O.; Yasukawa, K.; Ihle, J. N.; Kishimoto, T.; Taga, T. Activation of JAK2 kinase mediated by the interleukin 6 signal transducer gp130. *Proc. Natl. Acad. Sci. U. S. A.* **1994**, 91 (6), 2285–2289.
- (10) Guschin, D.; Rogers, N.; Briscoe, J.; Witthuhn, B.; Watling, D.; Horn, F.; Pellegrini, S.; Yasukawa, K.; Heinrich, P.; Stark, G. R.; Ihle, J. N.; Kerr, I. M. A major role for the protein tyrosine kinase JAK1 in the JAK/STAT signal transduction pathway in response to interleukin-6. *EMBO J.* **1995**, 14 (7), 1421–1429.
- (11) Ghoreschi, K.; Laurence, A.; O'Shea, J. J. Janus kinases in immune cell signaling. *Immunol. Rev.* **2009**, 228 (1), 273–287.
- (12) Pesu, M.; Laurence, A.; Kishore, N.; Zwillich, S. H.; Chan, G.; O'Shea, J. J. Therapeutic targeting of Janus kinases. *Immunol. Rev.* **2008**, 223, 132–142.
- (13) Vijaykrishnan, L.; Venkataramanan, R.; Gulati, P. Treating inflammation with the Janus kinase inhibitor CP-690,550. *Trends Pharmacol. Sci.* **2011**, 32 (1), 25–34.
- (14) Tefferi, A.; Pardanani, A. JAK inhibitors in myeloproliferative neoplasms: rationale, current data and perspective. *Blood Rev.* **2011**, 25 (5), 229–237.
- (15) Quintás-Cardama, A.; Kantarjian, H.; Cortes, J.; Verstovsek, S. Janus kinase inhibitors for the treatment of myeloproliferative neoplasias and beyond. *Nature Rev. Drug Discovery* **2011**, 10 (2), 127–140.
- (16) Kremer, J. M.; Bloom, B. J.; Breedveld, F. C.; Coombs, J. H.; Fletcher, M. P.; Gruben, D.; Krishnaswami, S.; Burgos-Vargas, R.; Wilkinson, B.; Zerbini, C. A.; Zwillich, S. H. The safety and efficacy of a JAK inhibitor in patients with active rheumatoid arthritis: Results of a double-blind, placebo-controlled phase IIa trial of three dosage levels of CP-690,550 versus placebo. *Arthritis Rheum.* **2009**, 60 (7), 1895–1905.
- (17) Fleischmann, R.; Cutolo, M.; Genovese, M. C.; Lee, E. B.; Kanik, K. S.; Sadis, S.; Connell, C. A.; Gruben, D.; Krishnaswami, S.;

Wallenstein, G.; Wilkinson, B. E.; Zwillich, S. H. Phase IIb dose-ranging study of the oral JAK inhibitor tofacitinib (CP-690,550) or adalimumab monotherapy versus placebo in patients with active rheumatoid arthritis with an inadequate response to disease-modifying antirheumatic drugs. *Arthritis Rheum.* **2012**, *64* (3), 617–629.

(18) Thoma, G.; Nuninger, F.; Falchetto, R.; Hermes, E.; Tavares, G. A.; Vangrevelinghe, E.; Zerwes, H.-G. Identification of a potent Janus kinase 3 inhibitor with high selectivity within the Janus kinase family. *J. Med. Chem.* **2011**, *54* (1), 284–288.

(19) Haan, C.; Rolvering, C.; Raulf, F.; Kapp, M.; Drückes, P.; Thoma, G.; Behrmann, I.; Zerwes, H.-G. Jak1 has a dominant role over Jak3 in signal transduction through γ c-containing cytokine receptors. *Chem. Biol.* **2011**, *18* (3), 314–323.

(20) Lin, T. H.; Hegen, M.; Quadros, E.; Nickerson-Nutter, C. L.; Appell, K. C.; Cole, A. G.; Shao, Y.; Tam, S.; Ohlmeyer, M.; Wang, B.; Goodwin, D. G.; Kimble, E. F.; Quintero, J.; Gao, M.; Symanowicz, P.; Wrocklage, C.; Lussier, J.; Schelling, S. H.; Hewet, A. G.; Xuan, D.; Krykbaev, R.; Toggias, J.; Xu, X.; Harrison, R.; Mansour, T.; Collins, M.; Clark, J. D.; Webb, M. L.; Seidl, K. J. Selective functional inhibition of JAK-3 is sufficient for efficacy in collagen-induced arthritis in mice. *Arthritis Rheum.* **2010**, *62* (8), 2283–2293.

(21) Goldstein, D. M.; Gray, N. S.; Zarrinkar, P. P. High-throughput kinase profiling as a platform for drug discovery. *Nature Rev. Drug Discovery* **2008**, *7* (5), 391–397.

(22) Fabian, M. A.; Biggs, I. I. I.; William, H.; Treiber, D. K.; Atteridge, C. E.; Azimioara, M. D.; Benedetti, M. G.; Carter, T. A.; Ciceri, P.; Edeen, P. T.; Floyd, M.; Ford, J. M.; Galvin, M.; Gerlach, J. L.; Grotzfeld, R. M.; Herrgard, S.; Insko, D. E.; Insko, M. A.; Lai, A. G.; Lelias, J.; Mehta, S. A.; Milanov, Z. V.; Velasco, A. M.; Wodicka, L. M.; Patel, H. K.; Zarrinkar, P. P.; Lockhart, D. J. A small molecule-kinase interaction map for clinical kinase inhibitors. *Nature Biotechnol.* **2005**, *23* (3), 329–336.

(23) Out of 293 wild-type kinases tested at Kinomescan, compound **2** at 10 μ M showed >90% bait ligand displacement for 156 kinases, including JAK1–3 (kinase domains) at the percentages indicated: JAK1 (100%), JAK2 (99%), and JAK3 (98%).

(24) Chrencik, J. E.; Patny, A.; Leung, I. K.; Korniski, B.; Emmons, T. L.; Hall, T.; Weinberg, R. A.; Gormley, J. A.; Williams, J. M.; Day, J. E.; Hirsch, J. L.; Kiefer, J. R.; Leone, J. W.; Fischer, H. D.; Himmers, C. D.; Huang, H.-C.; Jacobsen, E. J.; Tenbrink, R. E.; Tomasselli, A. G.; Benson, T. E. Structural and thermodynamic characterization of the TYK2 and JAK3 kinase domains in complex with CP-690550 and CMP-6. *J. Mol. Biol.* **2010**, *400* (3), 413–433.

(25) Flanagan, M. E.; Blumenkopf, T. A.; Brissette, W. H.; Brown, M. F.; Casavant, J. M.; Chang, S.-P.; Doty, J. L.; Elliott, E. A.; Fisher, M. B.; Hines, M.; Kent, C.; Kudlacz, E. M.; Lillie, B. M.; Magnuson, K. S.; McCurdy, S. P.; Munchhof, M. J.; Perry, B. D.; Sawyer, P. S.; Strelevitz, T. J.; Subramanyam, C.; Sun, J.; Whipple, D. A.; Changelian, P. S. Discovery of CP-690,550: a potent and selective Janus kinase (JAK) inhibitor for the treatment of autoimmune diseases and organ transplant rejection. *J. Med. Chem.* **2010**, *53* (24), 8468–8484.

(26) *Molecular Operating Environment (MOE)*, 2011.10; Chemical Computing Group Inc.: 1010 Sherbooke St. West, Suite #910, Montreal, QC, Canada, H3A 2R7, 2011.

(27) Tanaka, N.; Asao, H.; Ohbo, K.; Ishii, N.; Takeshita, T.; Nakamura, M.; Sasaki, H.; Sugamura, K. Physical association of Jak1 and Jak2 tyrosine kinases with the interleukin 2 receptor β and γ chains. *Proc. Natl. Acad. Sci. U. S. A.* **1994**, *91*, 7271–7275.

(28) Otwinowski, Z.; Minor, W. Processing of X-ray diffraction data collected in oscillation mode. In *Macromolecular Crystallography, Part A*; Carter, C. W. J., Sweet, R. M., Eds.; Academic Press: New York, 1997; pp 307–326.

(29) McCoy, A. J.; Grosse-Kunstleve, R. W.; Storoni, L. C.; Read, R. J. Likelihood-enhanced fast translation functions. *Acta Crystallogr., Sect. D: Biol. Crystallogr.* **2005**, *61*, 458–464.

(30) Boggon, T. J.; Li, Y.; Manley, P. W.; Eck, M. J. *Blood* **2005**, *106*, 996–1002.

(31) Murshudov, G. N.; Vagin, A. A.; Dodson, E. J. Refinement of macromolecular structures by the maximum-likelihood method. *Acta Crystallogr., Sect. D: Biol. Crystallogr.* **1997**, *53*, 240–255.

(32) Emsley, P.; Cowtan, K. Coot: Model-building tools for molecular graphics. *Acta Crystallogr., Sect. D: Biol. Crystallogr.* **2004**, *60*, 2126–2132.